SUPPORTING INFORMATION FOR:

Stable Double Gyroid Network Phases in Asymmetric Linear Triblock Amphiphiles

Daoyuan Li,[†,‡] Mahesh K. Mahanthappa,[†]

Timothy P. Lodge,[*,†,¶] and J. Ilja Siepmann[*,†,¶,‡]

†*Department of Chemical Engineering and Materials Science, University of Minnesota, 421 Washington Avenue SE, Minneapolis, Minnesota 55455-0132, United States*

‡ *Chemical Theory Center, University of Minnesota, 207 Pleasant Street SE, Minneapolis, Minnesota 55455-0431, United States*

¶ *Department of Chemistry, University of Minnesota, 207 Pleasant Street SE, Minneapolis, Minnesota 55455-0431, United States*

E-mail: lodge@umn.edu; siepmann@umn.edu

Force Field Details

The asymmetric $B_6A_4B_x$ triblock amphiphiles are modeled using the united-atom version of the transferable potentials for phase equilibria (TraPPE–UA) force field.[1–4] In this approach, CH_q groups are treated as single pseudo-atoms, while polar hydrogen atoms in hydroxyl groups are explicitly modeled with partial charges, albeit without Lennard-Jones (LJ) interactions. The relevant LJ parameters and partial charges for Coulomb interactions are detailed in Tables S1.

To regulate intramolecular hydrogen bonding between adjacent hydroxyl groups, a short-range repulsive potential is applied to 1-5 interactions between hydrogen and oxygen atoms belonging to separate hydroxyl groups that are connected via four bonds. These interactions exclude the 1–4 O–O LJ terms but incorporate scaled 1–4 Coulomb interactions with a scaling factor of 0.5.[3] The repulsive potential, $U_{\text{repulsive}}(r_{ij})$, is expressed as

$$\frac{U_{\text{repulsive}}(r_{ij})}{k_{\text{B}}} = \frac{7.5 \times 10^7 \text{ K} \cdot \text{Å}^{12}}{r_{ij}^{12}},$$

where r_{ij} represents the 1–5 separation between oxygen and hydrogen atoms.

Bonded interactions are described by parameters provided in Table S2. The potential functions employed are as follows:

$$u_{\text{stretching}}(r) = \frac{k_{\text{s}}}{2}(r - r_0)^2,$$

$$u_{\text{bending}}(\theta) = \frac{k_{\text{b}}}{2}(\theta - \theta_0)^2,$$

$$u_{\text{torsion}}(\phi) = c_0 + c_1[1 + \cos(\phi)] + c_2[1 - \cos(2\phi)] + c_3[1 + \cos(3\phi)].$$

While the standard TraPPE-UA force field utilizes rigid bond lengths that are suitable for Monte Carlo simulations, molecular dynamics simulations can be run more efficiently by allowing fluctuations in C–C and C–O bonds, with bond-stretching constants taken from the OPLS force field,[5] whereas O–H bonds remain constrained (to avoid affecting the strength

of hydrogen bonds). Bending and torsional parameters are adopted directly from TraPPE–UA.[1–4]

Calculation of Structure Factors

The structure factor $S(\mathbf{q})$ is computed using the following expression:

$$S(\mathbf{q}) = \frac{\left[\sum_{j=1}^{N_{\text{site}}} f_j(\mathbf{q}) \cos(\mathbf{q} \cdot \mathbf{r}_j)\right]^2 + \left[\sum_{j=1}^{N_{\text{site}}} f_j(\mathbf{q}) \sin(\mathbf{q} \cdot \mathbf{r}_j)\right]^2}{\sum_{j=1}^{N_{\text{site}}} f_j^2(\mathbf{q})},$$

where $\mathbf{q}$ denotes the scattering wave vector, $\mathbf{r}_j$ the position of the jth interaction site, and N_{site} the total number of such sites in the simulation box. The atomic form factor $f_j(\mathbf{q})$ is a function of $|\mathbf{q}|$; for CH_q pseudo-atoms, the form factor for carbon is used, while for hydroxyl groups, the individual form factors for oxygen and hydrogen are employed. These form factors are obtained from the International Tables for Crystallography.[6]

The accessible wave vectors within the simulation box are given by

$$\mathbf{q} = \frac{2\pi n_x}{L_x}\mathbf{e}_x + \frac{2\pi n_y}{L_y}\mathbf{e}_y + \frac{2\pi n_z}{L_z}\mathbf{e}_z,$$

where L_x, L_y, and L_z represent the box dimensions in the x, y, and z directions, and $\mathbf{e}_x$, $\mathbf{e}_y$, and $\mathbf{e}_z$ are the corresponding unit vectors (e.g., $\mathbf{e}_x = [1, 0, 0]$ in an orthorhombic system).

To expedite the large-scale matrix computations required for evaluating $S(\mathbf{q})$, parallel processing is implemented on both multi-core CPUs and GPUs using the Taichi programming language embedded in Python.[7–9] The final reported $S(\mathbf{q})$ values are averaged over all vectors sharing the same $|\mathbf{q}|$, and uncertainties are expressed as 95% confidence intervals.

Supplementary Tables

Table S1. Lennard-Jones parameters and partial charges for interaction sites

interaction site	σ [Å]	ϵ/k_B [K]	q [|e|]
CH_3	3.75	98	0
CH_x-**CH_2**-CH_x	3.95	46	0
CH_x-**CH_2**-O-H	3.95	46	0.265
$(CH_x)_2$-**CH**-O-H	4.33	10	0.265
O	3.02	93	−0.700
H	N/A	N/A	0.435

Table S2. Parameters for fixed bond lengths, harmonic bond bending potentials, and cosine series dihedral potentials

stretching	r_0 [Å]	$k_\mathrm{s}/k_\mathrm{B}[K]$		
CH_x-CH_y	1.54	270000		
CH_x-O	1.43	320000		
O-H	0.945	constrained		
bending	ϕ_0 [°]	$k_\mathrm{b}/k_\mathrm{B}$ [K]		
CH_x-(CH_2)-CH_y	114	62500		
CH_x-(CH)-CH_y	112	62500		
CH_x-(O)-H	108.5	55400		
CH_x-(CH)-O	109.5	50400		
torsion	c_0/k_B [K]	c_1/k_B [K]	c_1/k_B [K]	c_1/k_B [K]
CH_x-CH_2-CH_2-CH_y	0	355.03	−68.19	791.32
CH_x-CH_x-CH-CH_y	−251.06	428.73	−111.85	441.27
CH_x-CH_2-O-H	0	209.82	−29.17	187.93
CH_x-CH-O-H	215.89	197.33	31.46	−173.92

Supplementary Figures

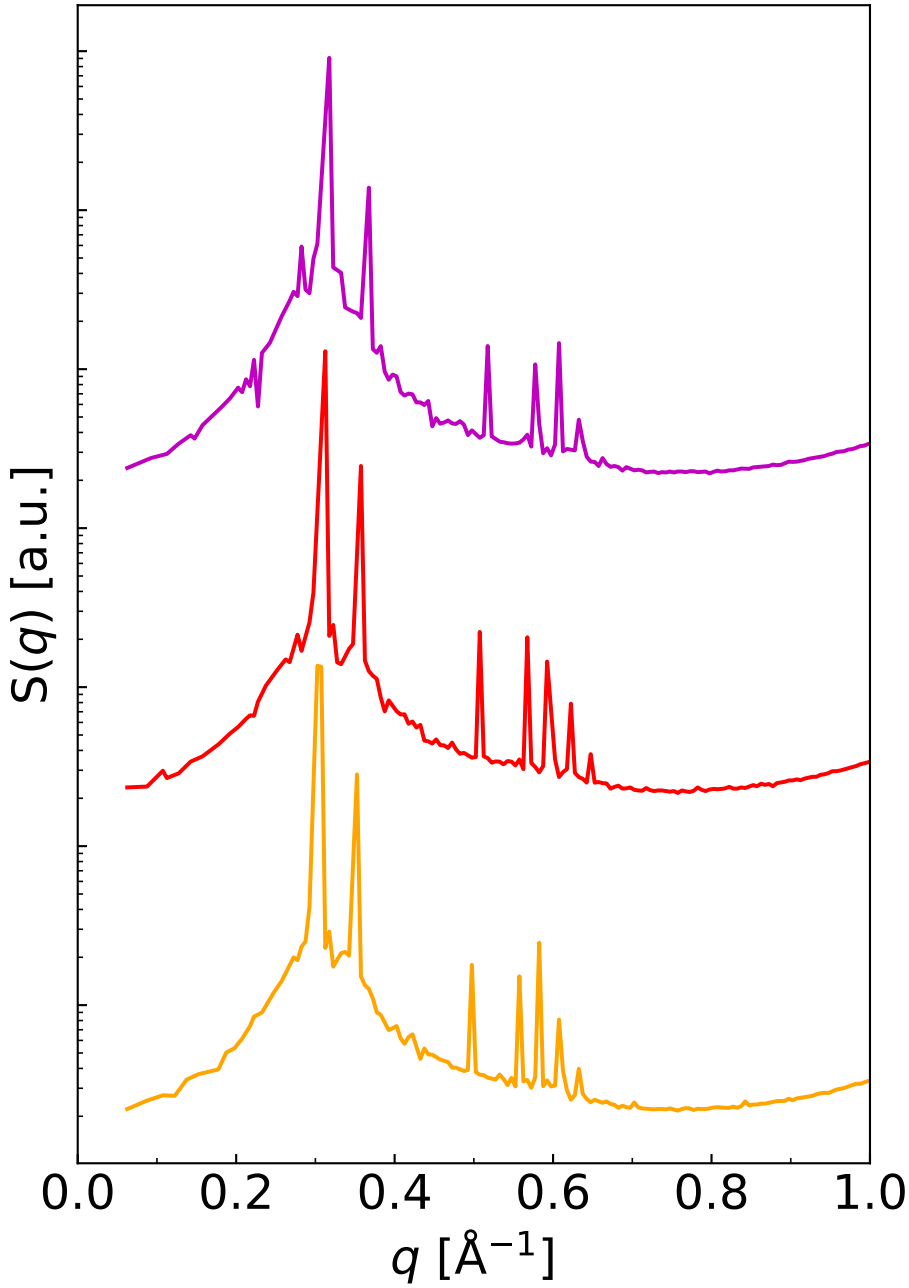

Figure S1. Static structure factors $S(q)$ of $B_6A_4B_9$ amphiphile systems: purple, red, and orange lines show data from simulations using $N = 1448$, 1544, and 1640 molecules, respectively.

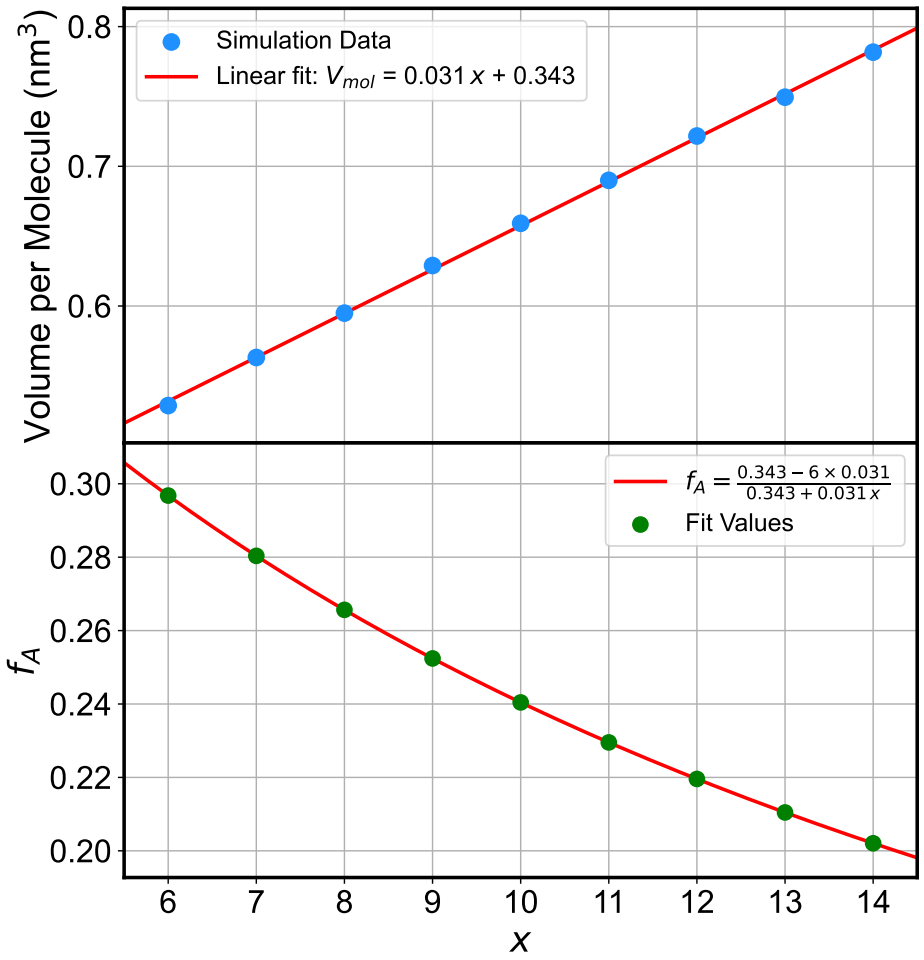

Figure S2. Molecular volumes (top) and volume fraction of the hydrophilic part (bottom) in $B_6A_4B_x$ as a function of x. The red line is a linear fit of the molecular volume data which can be used to estimate the volume occupied by the A_4 and the corresponding volume fraction.

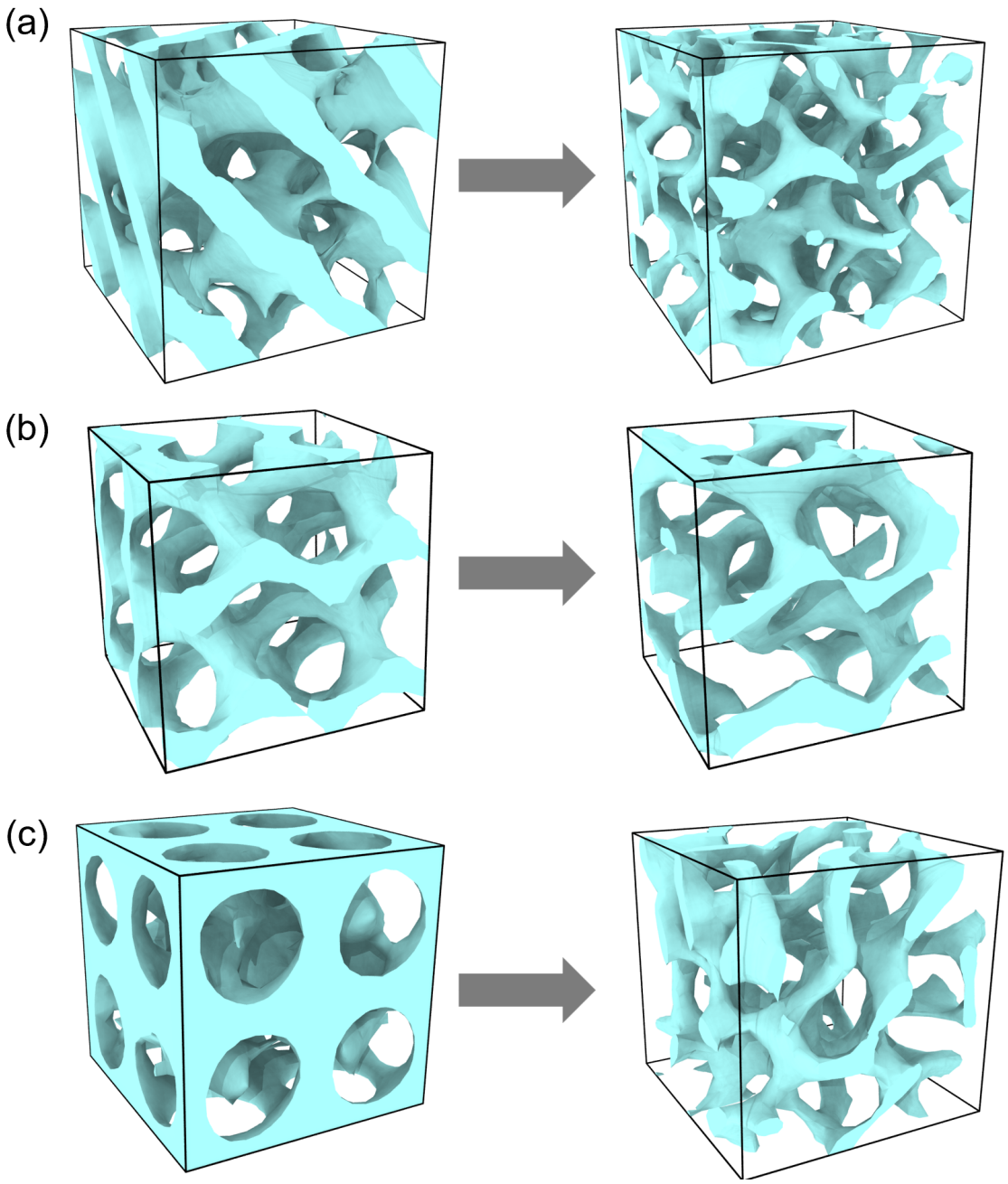

Figure S3. Dividing-surface snapshots: (a) double diamond, (b) single gyroid, (c) plumber's nightmare (double primitive) structures assembled via system-size tuning and guiding fields for $B_6A_4B_7$. The images on the left show the system immediately after removal of the guiding field and those on the right indicate the rapid transition to disordered structures within 50 ns upon removal of the guiding field.

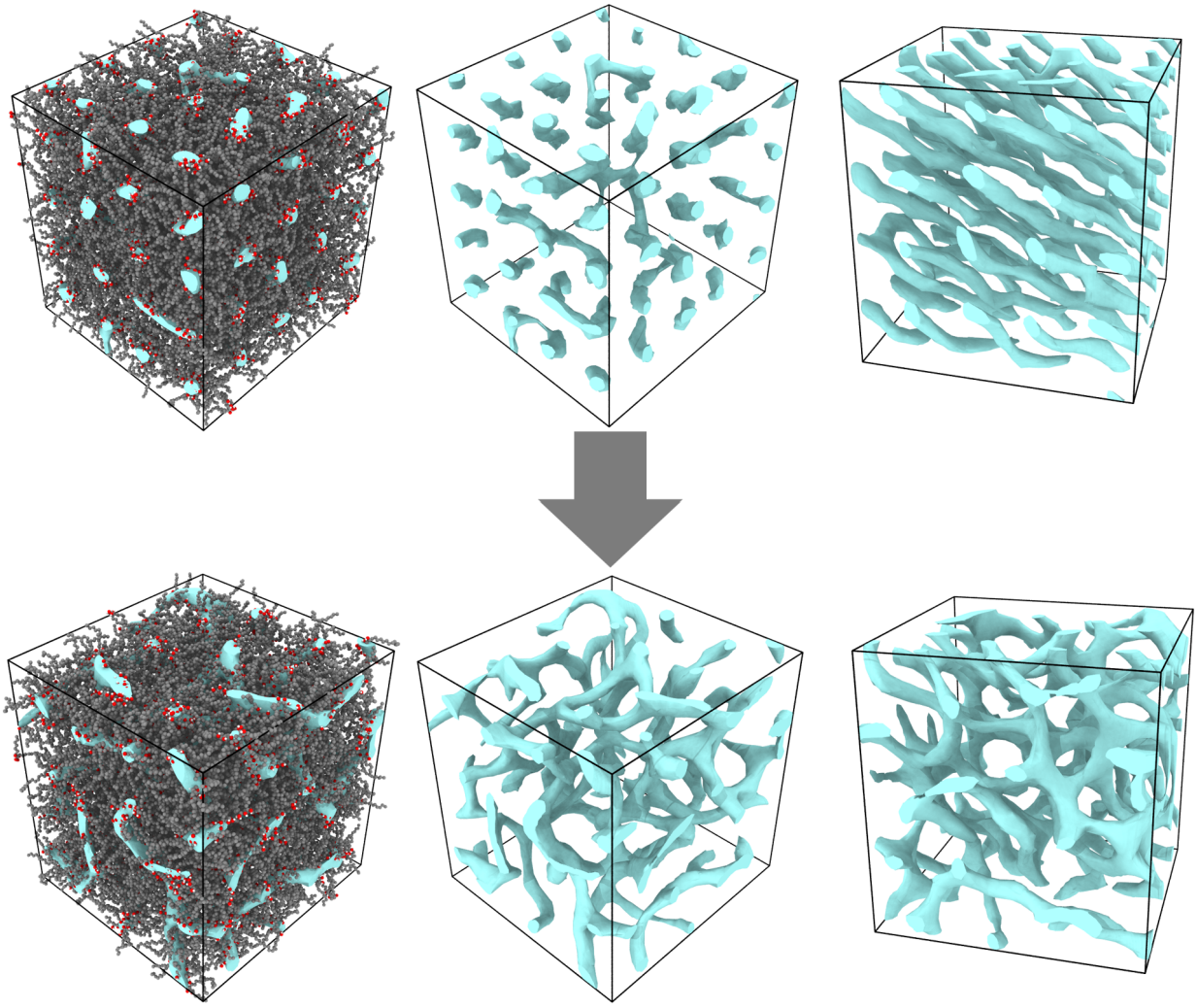

Figure S4. Dividing-surface snapshots with and without molecules for $B_6A_4B_{14}$. The initial hexagonally packed cylinder structure is found to evolve into a disordered structure after 50 ns.

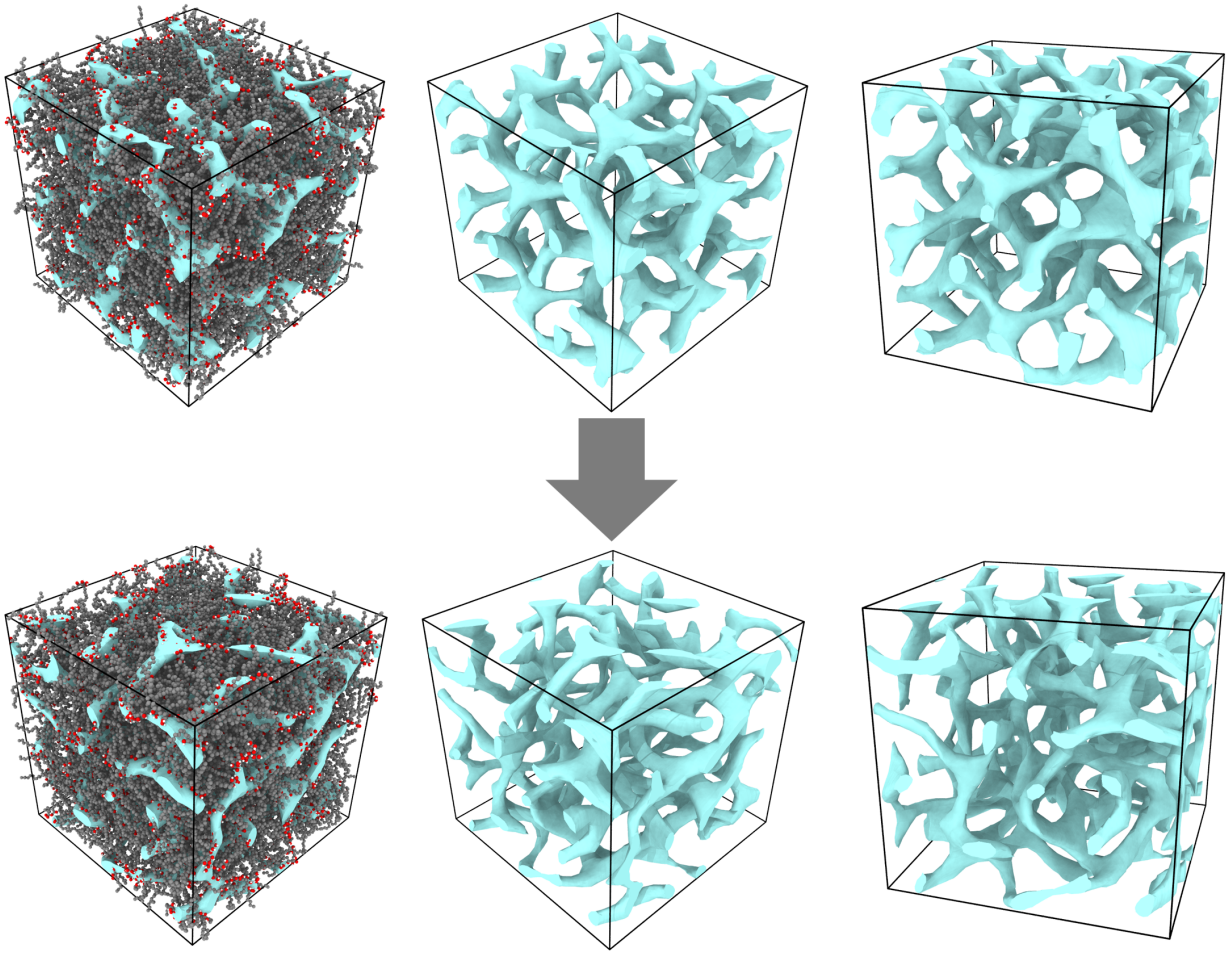

Figure S5. Dividing-surface snapshots with and without molecules for $B_6A_4B_{13}$. The initial double gyroid structure (top) is found to evolve into a disordered structure after 150 ns.

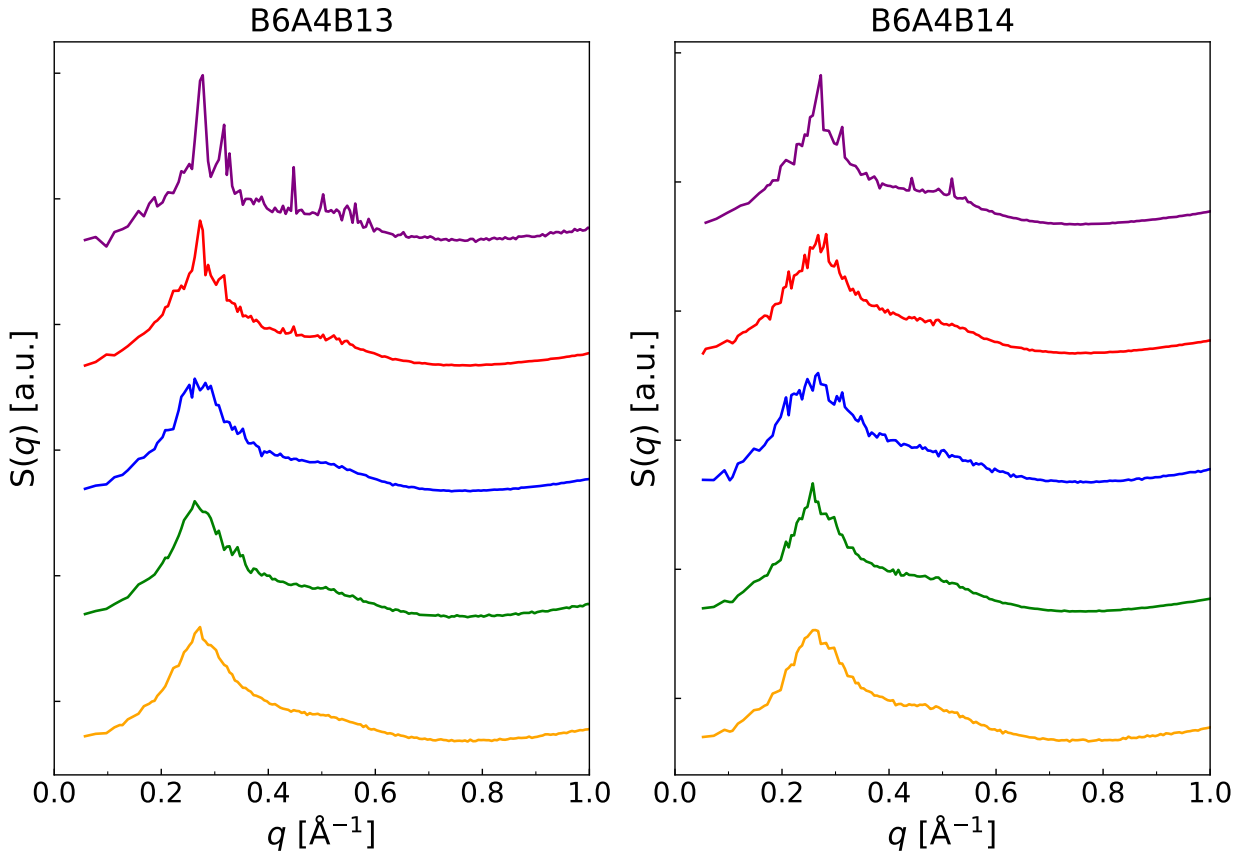

Figure S6. Static structure factors of the $B_6A_4B_{13}$ and $B_6A_4B_{14}$ simulations started from pre-assembled double gyroid structures calculated separately over (top to bottom) the 20–50, 50–100, 100–150, 900–1000, and 1900-2000 ns intervals.

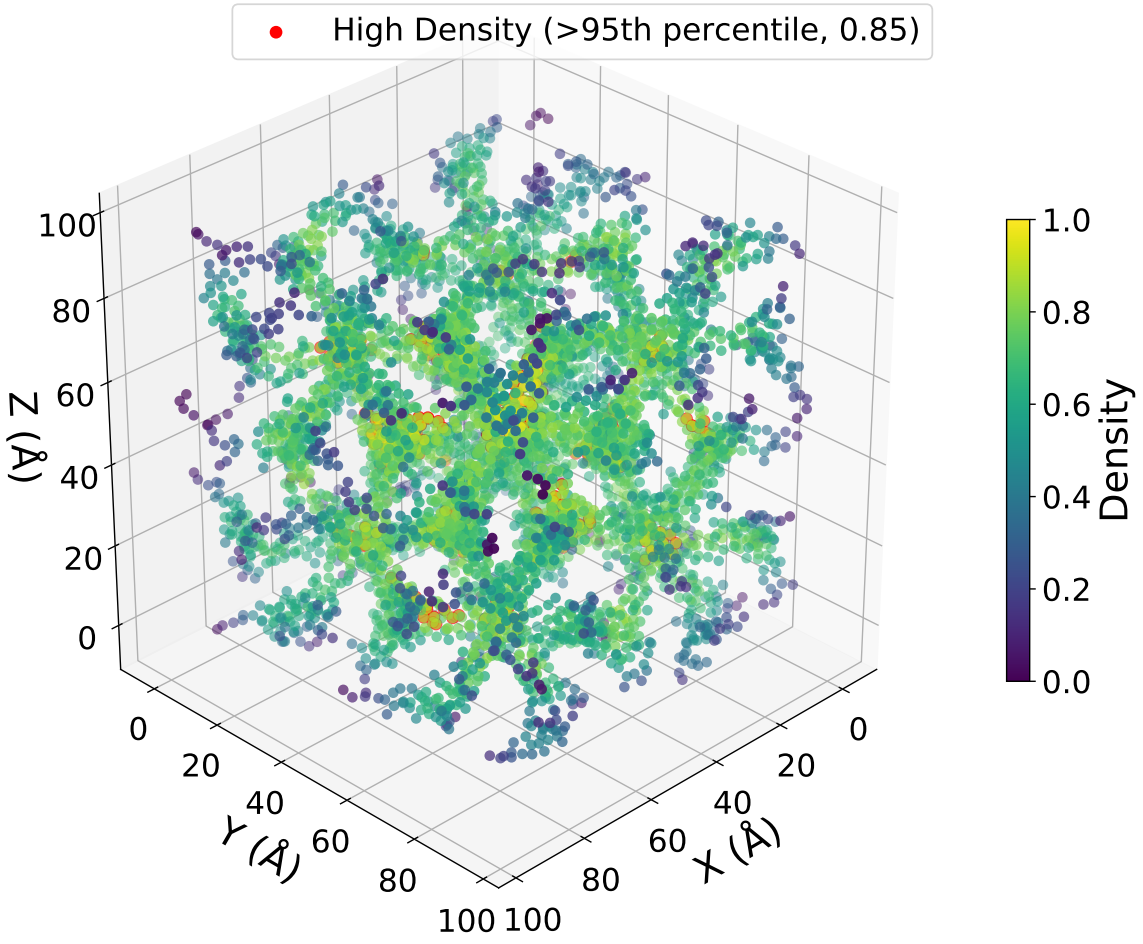

Figure S7. Positions of oxygen atom coordinates with relative density values derived from three-dimensional kernel density estimation for $B_6A_4B_7$. Points with densities above the 95th percentile of the overall distribution are highlighted in red as high-density points, corresponding to normalized density values from 0.85 to 1.

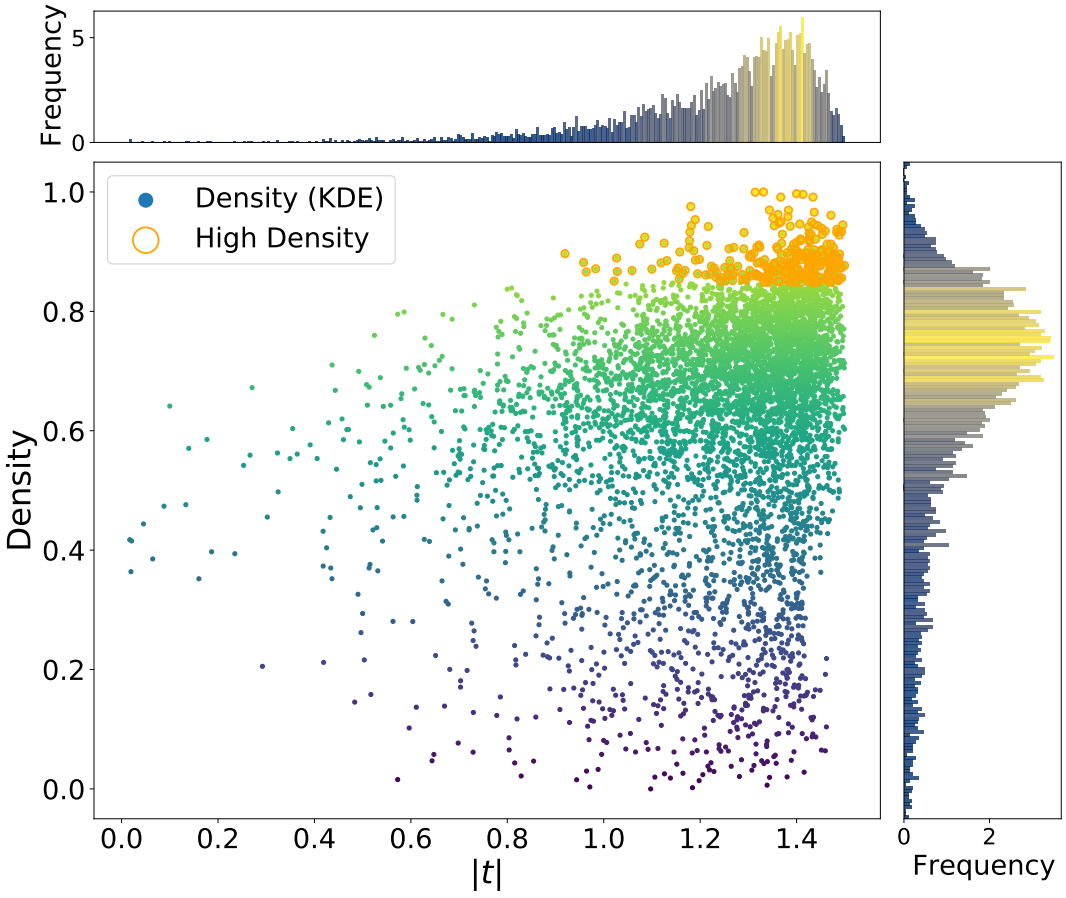

Figure S8. Scatter plot of $|t|$ values (from level surface analysis) as a function of oxygen atom coordinate densities from three-dimensional kernel density estimation for $B_6A_4B_7$. Points above the 95th percentile are highlighted in orange, corresponding to normalized density values from 0.85 to 1. Histograms along the top and right sides of the plot show the distributions of $|t|$ values and densities, with bar heights represented by gradient colors. Most oxygen atom coordinates cluster in the upper-right region, indicating that high-density points are concentrated at the center of the gyroid channels.

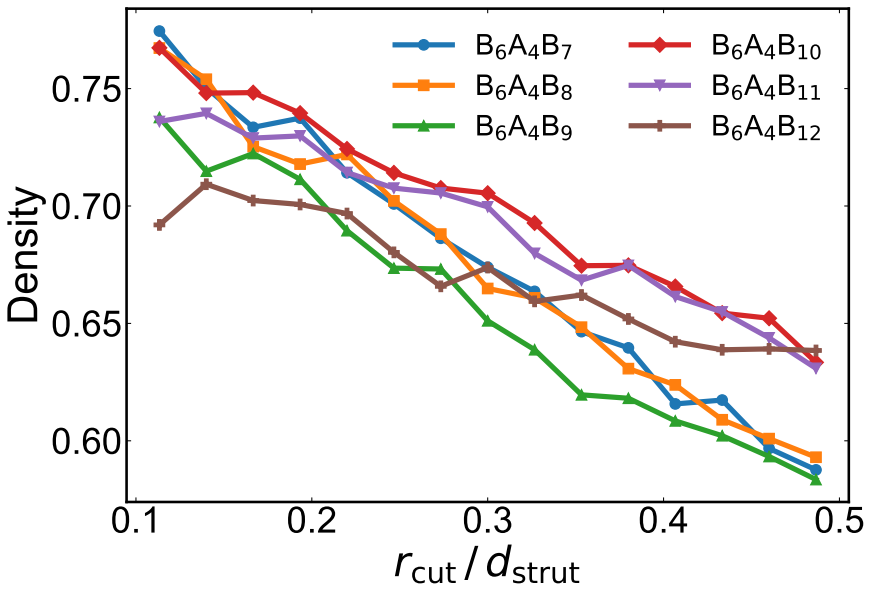

Figure S9. Normalized density of oxygen atom coordinates as a function of cutoff distance for $B_6A_4B_x$ amphiphiles.

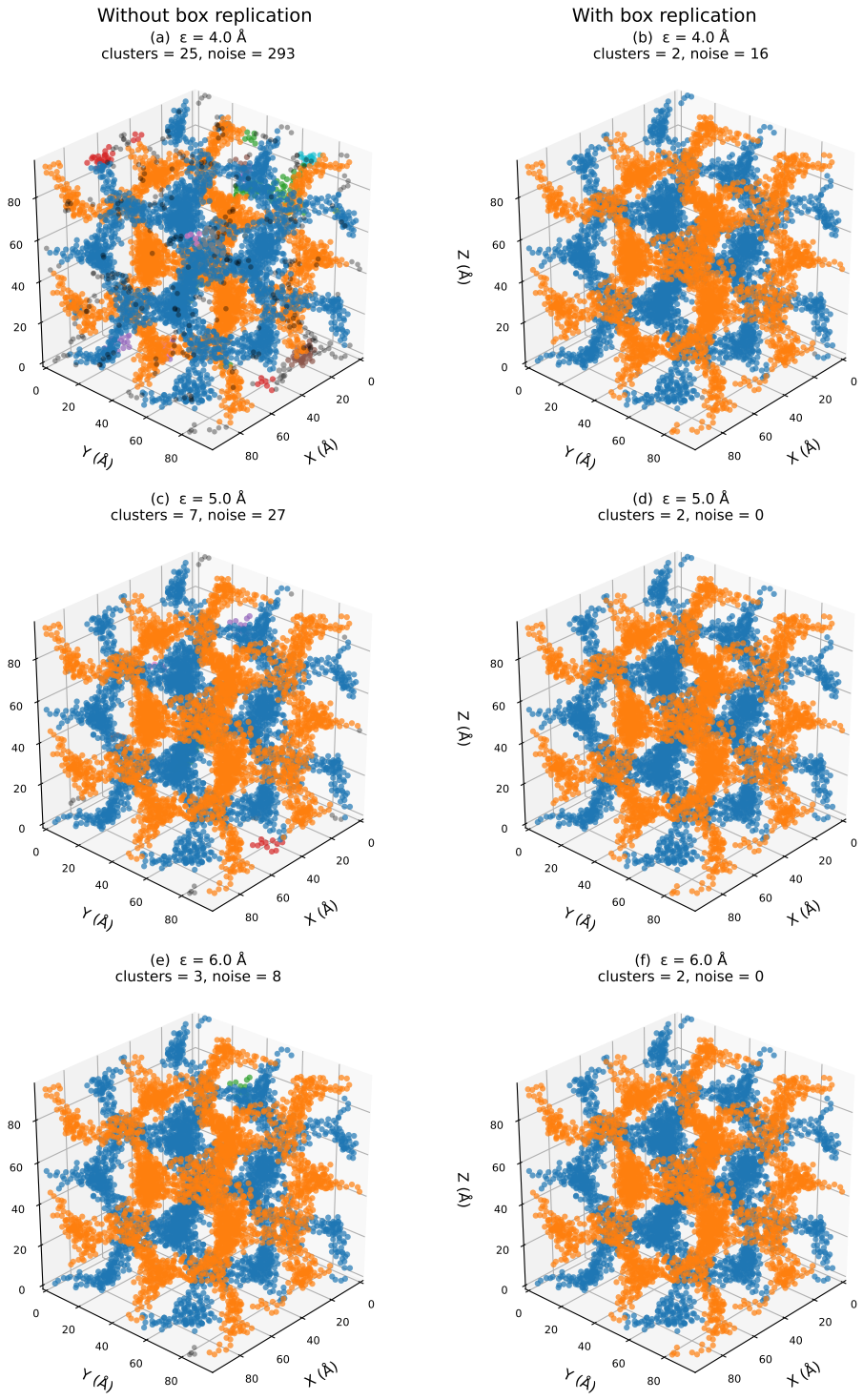

Figure S10. Sensitivity of the DBSCAN cluster assignment for the $B_6A_4B_8$ system with double gyroid morphology to the choice of the neighborhood radius, ε. The left column shows the clustering results obtained without box replication, and the right column shows the corresponding results obtained with $3 \times 3 \times 3$ box replication to account for periodic boundary conditions. The three rows correspond to $\varepsilon = 4.0$, 5.0, and 6.0 Å, respectively, with min_samples = 5 in all cases.

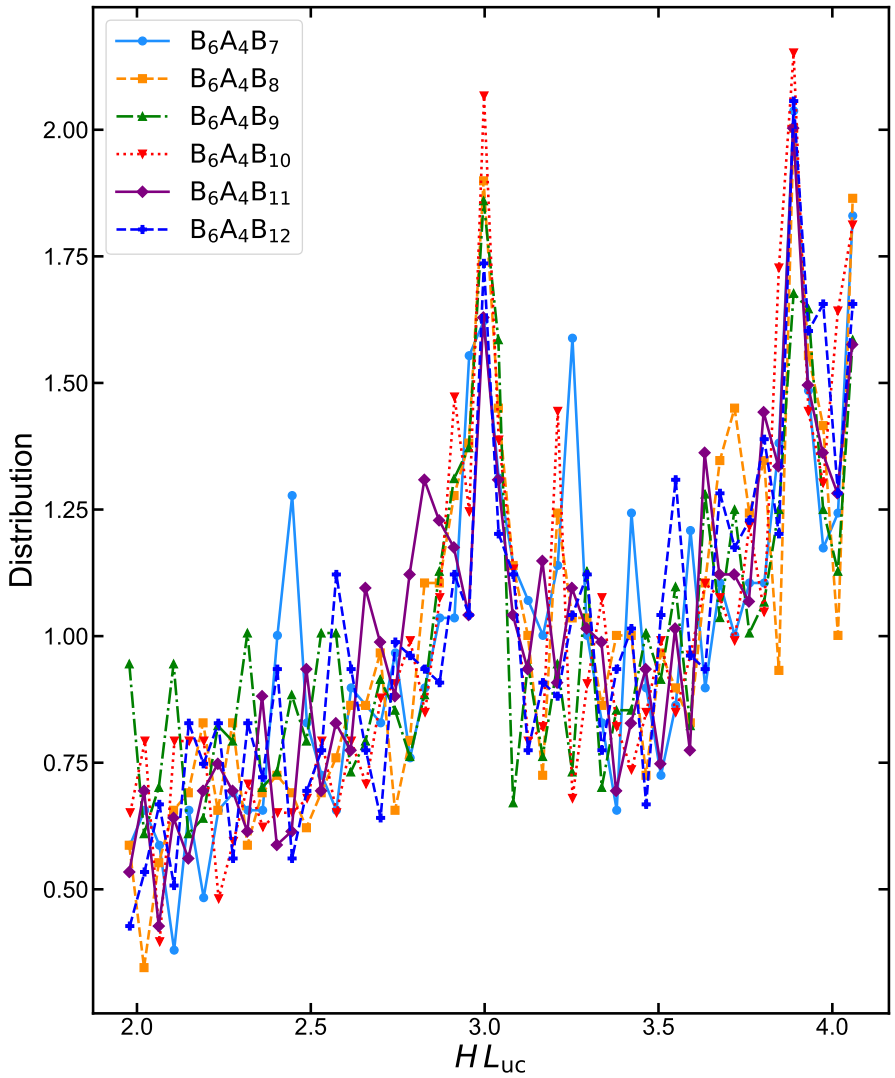

Figure S11. Distribution of $H\,L_{\mathrm{uc}}$ evaluated at the centers of the second and third hydroxyl carbons of DG-forming $B_6A_4B_x$ amphiphiles ($x = 7$–12).

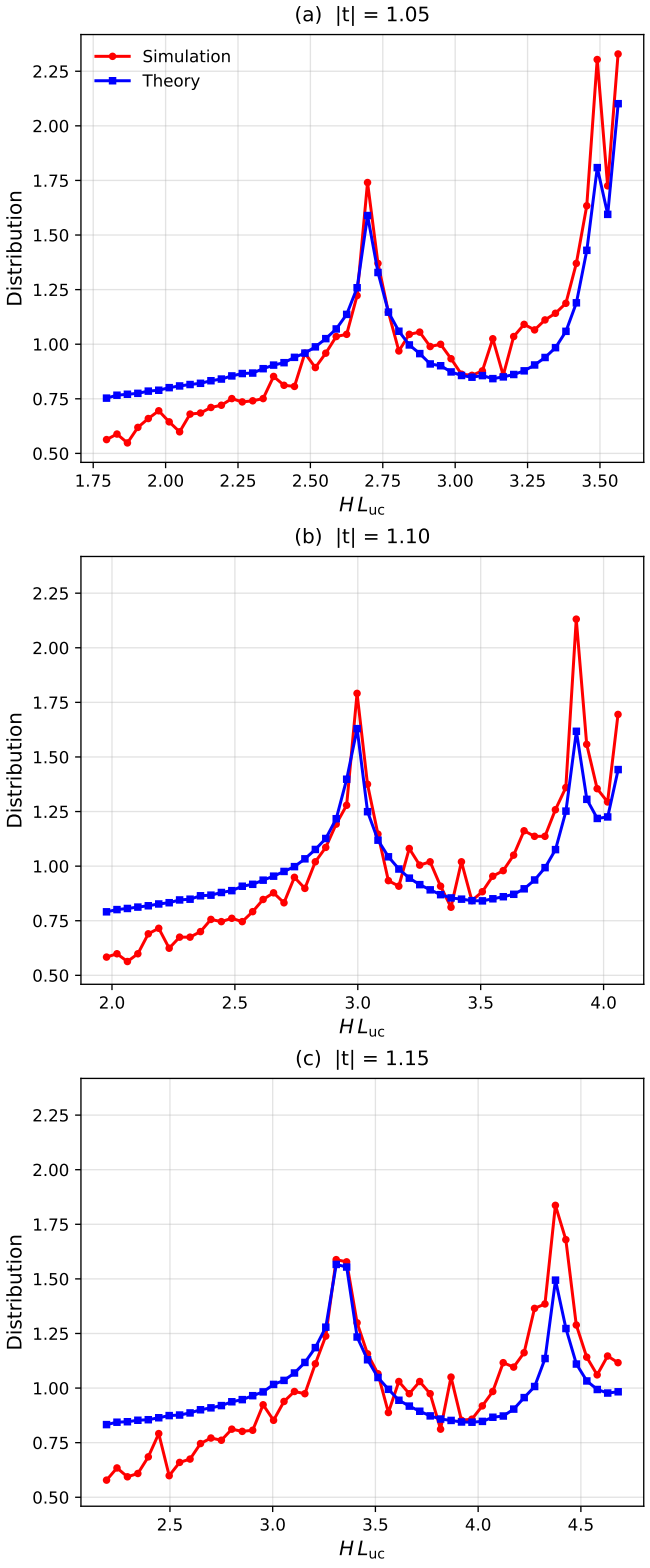

Figure S12. Sensitivity of the curvature-distribution analysis to the choice of the implicit gyroid level-set constant, $|t|$. The three panels show the comparison between the simulation-derived and theoretical curvature distributions for $|t| = 1.05$, 1.10, and 1.15.

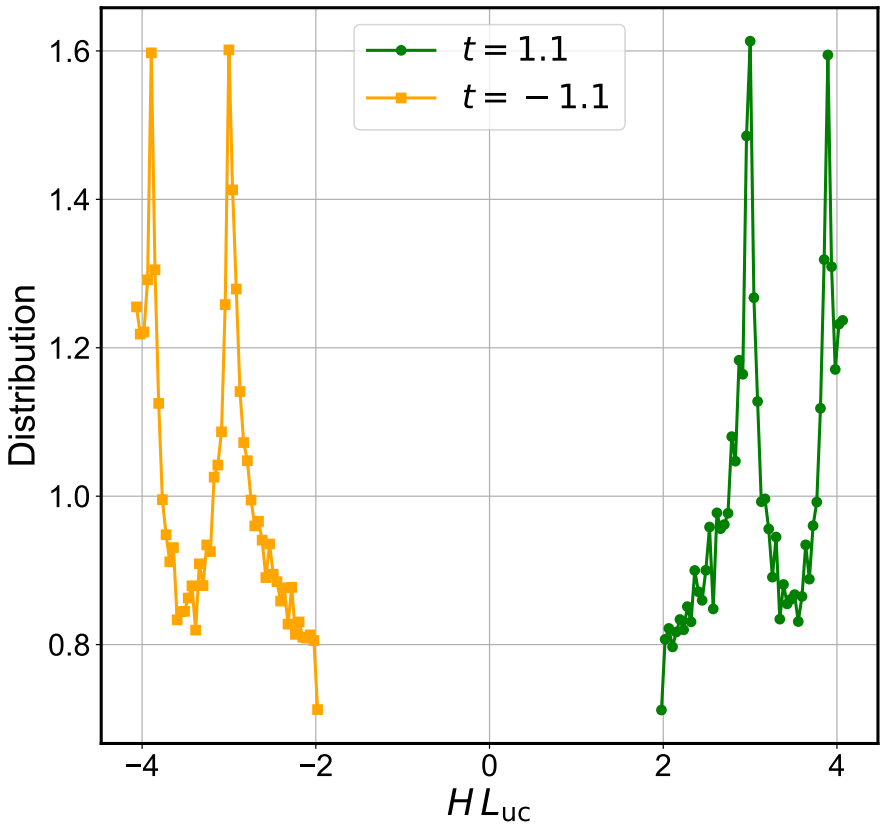

Figure S13. Distribution of $H\,L_{\mathrm{uc}}$ with the conventional definition of the surface normal.

References

(1) Martin, M. G.; Siepmann, J. I. Transferable Potentials for Phase Equilibria. 1. United-Atom Description of n-Alkanes. *J. Phys. Chem. B* **1998**, *102*, 2569–2577.

(2) Martin, M. G.; Siepmann, J. I. Novel Configurational-Bias Monte Carlo Method for Branched Molecules. Transferable Potentials for Phase Equilibria. 2. United-Atom Description of Branched Alkanes. *J. Phys. Chem. B* **1999**, *103*, 4508–4517.

(3) Chen, B.; Potoff, J. J.; Siepmann, J. I. Monte Carlo Calculations for Alcohols and Their Mixtures with Alkanes. Transferable Potentials for Phase Equilibria. 5. United-Atom Description of Primary, Secondary, and Tertiary Alcohols. *J. Phys. Chem. B* **2001**, *105*, 3093–3104.

(4) Stubbs, J. M.; Potoff, J. J.; Siepmann, J. I. Transferable Potentials for Phase Equilibria. 6. United-Atom Description for Ethers, Glycols, Ketones, and Aldehydes. *J. Phys. Chem. B* **2004**, *108*, 17596–17605.

(5) Jorgensen, W. L.; Maxwell, D. S.; Tirado-Rives, J. Development and Testing of the OPLS All-Atom Force Field on Conformational Energetics and Properties of Organic Liquids. *J. Am. Chem. Soc.* **1996**, *118*, 11225–11236.

(6) Prince, E. *International Tables for Crystallography, Volume C: Mathematical, Physical and Chemical Tables*; Springer Science & Business Media, 2004.

(7) Hu, Y.; Li, T.-M.; Anderson, L.; Ragan-Kelley, J.; Durand, F. Taichi: A Language for High-Performance Computation on Spatially Sparse Data Structures. *ACM Trans. Graph.* **2019**, *38*, 1–16.

(8) Hu, Y.; Anderson, L.; Li, T.-M.; Sun, Q.; Carr, N.; Ragan-Kelley, J.; Durand, F. Difftaichi: Differentiable Programming for Physical Simulation. *arXiv Preprint arXiv:1910.00935* **2019**,

(9) Hu, Y.; Liu, J.; Yang, X.; Xu, M.; Kuang, Y.; Xu, W.; Dai, Q.; Freeman, W. T.; Durand, F. Quantaichi: A Compiler for Quantized Simulations. *ACM Trans. Graph.* **2021**, *40*, 1–16.